Preparation and characterization of copper catalysts supported on mesoporous Al_2O_3 nanofibers for N_2O reduction to N_2

Z.H. Zhu[a,*], H.Y. Zhu[b], S.B. Wang[a], and G.Q. Lu[b]

[a]*Department of Chemical Engineering, Curtin University of Technology, GPO Box, U1987, Perth 6845, Australia*
[b]*Nanomaterials Centre, The University of Queensland, QLD 4072, Australia*

Received 27 June 2003; accepted 2 September 2003

A series of mesoporous Al_2O_3 samples with different porous structures and phases were prepared and used as supports for Cu/Al_2O_3 catalysts. These catalysts were characterized by N_2 adsorption, NMR, TGA, XRD, and UV–vis spectroscopic techniques and tested for the catalytic reaction of N_2O decomposition. The activity increased with the increasing calcination temperatures of supports from 450 to 900 °C; however, a further increase in calcination temperature up to 1200 °C resulted in a significant reduction in activity. Characterization revealed that the calcination temperatures of supports influenced the porous structures and phases of the supports, which in turn affected the dispersions, phases, and activities of the impregnated copper catalyst. The different roles of surface spinel, bulk $CuAl_2O_4$, and bulk CuO is clarified for N_2O catalytic decomposition. Two mechanism schemes were thus proposed to account for the varying activities of different catalysts.

KEY WORDS: mesoporous alumina; copper catalysts; N_2O decomposition.

1. Introduction

Cu/Al_2O_3 are important catalysts for many catalytic reactions. The investigation of Cu/Al_2O_3 catalysts by Friedman *et al.* [1] found that a number of γ-aluminas appeared to have a similar threshold loading for the appearance of crystalline CuO, ca. 4 wt% $Cu/100\,m^2/g$-support, below which "surface spinel" (which "resembles" $CuAl_2O_4$) (at very low loading) and bulk $CuAl_2O_4$ (at relatively higher loading) predominated copper phases in catalysts at calcination temperature below 500 °C.

Strohmeier *et al.* [2] also found that the surface characteristics of the catalysts were affected by both metal loading and calcination temperature. However, the site symmetry of Cu^{2+} ions (CuO-square planar; $CuAl_2O_4$—60% tetrahedral Td, 40% octahedral Oh; Cu/Al_2O_3 interaction species—predominantly Oh) has little effect on the reduction by H_2 and sulfidation with 15% H_2S/H_2, in contrast to the Co/Al_2O_3 and Ni/Al_2O_3 system [3,4].

Hierl *et al.* [5] conducted a comparative study of CuO/Al_2O_3 and $CuO\text{-}NiO/Al_2O_3$. They concluded that Ni^{2+} ions have a strong tendency to occupy octahedral sites in subsurface layers and in the bulk. The presence of Ni^{2+} led to Cu^{2+} redistribution with an increasing population of Cu^{2+} occupying tetrahedral sites. Once again, Cu^{2+} was found to be more readily reduced than Ni^{2+} by H_2 or vacuum heat treatment.

* To whom correspondence should be addressed.
E-mail: Zhuz@vesta.curtin.edu.au

The CuO species supported on γ-Al_2O_3 were further classified by Tikhov *et al.* [6] as isolated ions, weak magnetic associates, two- and three-dimensional clusters, and defected CuO phase. The most reactive sites in reduction by CO were found to be three-dimensional clusters. In a follow-up study, Dow *et al.* [7] investigated the temperature-programmed reduction (TPR) of supported CuO in hydrogen. They reported that two TPR peaks were observed. The peak at low temperature was attributed to the reduction of highly dispersed copper oxides; the peak at high temperature was ascribed to the reduction of bulk CuO (big three-dimensional clusters). The highly dispersed copper oxide species contained isolated copper ions, weak magnetic associates, and small two- and three-dimensional clusters.

In the study of Cu/γ-Al_2O_3 for NO reduction by C_3H_6, Shimizu [8] found that 8 wt% Cu/Al_2O_3 was more active after calcination at higher temperature (800 °C) than at lower temperature (400 °C). For NO reduction, they attributed the higher activity of Cu/Al_2O_3 to the surface aluminate phase, which contains highly dispersed transition metal cations in Al_2O_3 matrix. A study on N_2O decomposition over grafted CuO/γ-Al_2O_3 catalysts was conducted by Yao *et al.* [9]. By repeating grafting reactions, complete layers were formed. The first grafting step was found to result in isolated copper ion centers, which were of very low activity. The specific activity of the catalyst remained unchanged after the second grafting step. Only after the third grafting, the catalytic activity normalized per copper ion in the surface increased about 4–6 fold. They then concluded that isolated copper ions are much

1011-372X/03/1100–0073/0

less active than paired copper ions. This is contrary to the case of Cr_2O_3/α-Al_2O_3, in which isolated Cr^{3+} ions were shown to be more active than paired Cr^{3+} ions [10]. In both cases, the reason the isolated and paired ions have different activities was not clarified.

The previous work concentrated on the effects of loading and calcination of catalysts on the properties of catalysts. However, no detailed study has appeared about the influences of the pore structures and phases of the parent Al_2O_3 supports on the activities of catalysts. The mechanism of N_2O catalytic decomposition over Al_2O_3 supported catalysts is yet to be clarified. In this work, a series of Al_2O_3 supports were prepared by heating boehmite nanofibers at different temperatures. We aim to study the influence of the pore structures and the phase transition of the parent supports on the catalytic performance of Cu/Al_2O_3 catalysts. We also aim to clarify the different active sites of these prepared catalysts in the catalytic decomposition of N_2O.

2. Experimental

2.1. Preparation of Al_2O_3 supports and catalysts

A $NaAlO_2$ solution was added dropwise into 5 N acetic acid solution under vigorous stirring. A white precipitate was formed and separated by centrifugation, and washed 3–4 times to remove Na^+ ions. The nonionic polyethylene oxide (PEO) surfactant, Tergitol 15S-7($C_{12-14}H_{25-29}O(CH_2CH_2O)_7H$) obtained from Aldrich, was mixed with the washed precipitate at a predetermined molar ratio of surfactant to aluminium (PEO/Al) and stirred for 2 h. The mixture was transferred into an autoclave and maintained at 100 °C for 2 days. A wet cake was recovered and dried in air. One portion of the samples (about 2.0 g) was calcined at 450 °C for 20 h, the second portion was calcined at 600 °C for 8 h, and two other portions were heat-treated at 900 °C and 1200 °C for 3 h, respectively. The temperature was raised at rate of 2 °C/min, starting from 100 °C. The four prepared Al_2O_3 samples were thus designated as Al_2O_3-450, Al_2O_3-600, Al_2O_3-900, and Al_2O_3-1200, respectively. The catalysts were prepared by impregnating the above four Al_2O_3 samples with an aqueous solution of copper nitrate (BDH Chemicals) at room temperature, followed by drying at 100 °C and calcination at 300 °C in helium for 1 h. The loading of 5 wt% copper on these supports was kept.

2.2. Characterization

The BET surface areas and textural structure were determined by nitrogen adsorption–desorption isotherms using a NOVA 1200 adsorption analyzer (Quantachrome, USA). Before adsorption all the samples were degassed for 4 h at 300 °C. The surface areas were calculated using the BET model and internal and external pore volumes were derived from *t*-method [11]. The dispersion of copper on the catalysts was measured by N_2O chemisorptions carried out in a thermogravimetric analyzer (Shimadzu TGA-50). The sample was treated at 300 °C in 10% H_2/He for 5 h and then the temperature was cooled down to 90 °C followed by N_2O chemisorption. More details can be seen in the literature [12].

X-ray diffraction (XRD) patterns of the samples were measured on a Philips PW 1050/25 goniometer equipped with a graphite monochromator. Cu Kα radiation and a fixed power source (40 kV, 40 mA) were used. The scan rate was 1° (2θ)/min. The ^{27}Al MAS NMR spectra were recorded at a frequency of 78.205 MHz and a spinning rate of 8 kHz with a pulse length of 4 μs, a pulse interval of 1 s and approximately 10 000 scans. ^{27}Al chemical shifts are reported relative to 1 M $Al(NO_3)_3$ solution. Diffuse reflectance spectra in the ultraviolet-visible range (DR-UV–vis) were recorded between 200 and 900 nm with a JASCO 550 UV–vis spectrophotometer equipped with a JASCO ISV-469 integrating sphere. The absolute remittance R_∞ from the sample was measured. Relative remittance quantity $R'_\infty = R'_\infty$ (sample)/R_∞ (reference) was used to calculate the Kubelk–Munk function defined as $F(R_\infty)$ [13]

$$F(R_\infty) = (1–R)^2/R_\infty$$

The parent Al_2O_3 sample was used as a reference for the catalysts.

2.3. Catalytic activity test

The reaction of N_2O decomposition was carried out at atmospheric pressure in a fixed-bed flow reactor (10 mm ID) packed with 300-mg samples. The reactant gas (1.05% N_2O/He) was fed at a flow rate of 40 mL/min. The reaction temperature was maintained at 475 °C. The gaseous products were analyzed by a gas chromatograph (Shimadzu GC-17A) equipped with a thermal conductivity detector and a Carbosphere packed column.

3. Results

3.1. Pore structures of the Al_2O_3 supports

The N_2 adsorption isotherms of the various Al_2O_3 supports are presented in figure 1(a). The isotherms for both Al_2O_3-450 and Al_2O_3-600 show typical of type IV, which is the characteristic of mesoporous solids [14], except that the adsorption volume on the former Al_2O_3 is slightly higher. A typical IV isotherm is also observed on Al_2O_3-900, but the adsorption volume is quite low.

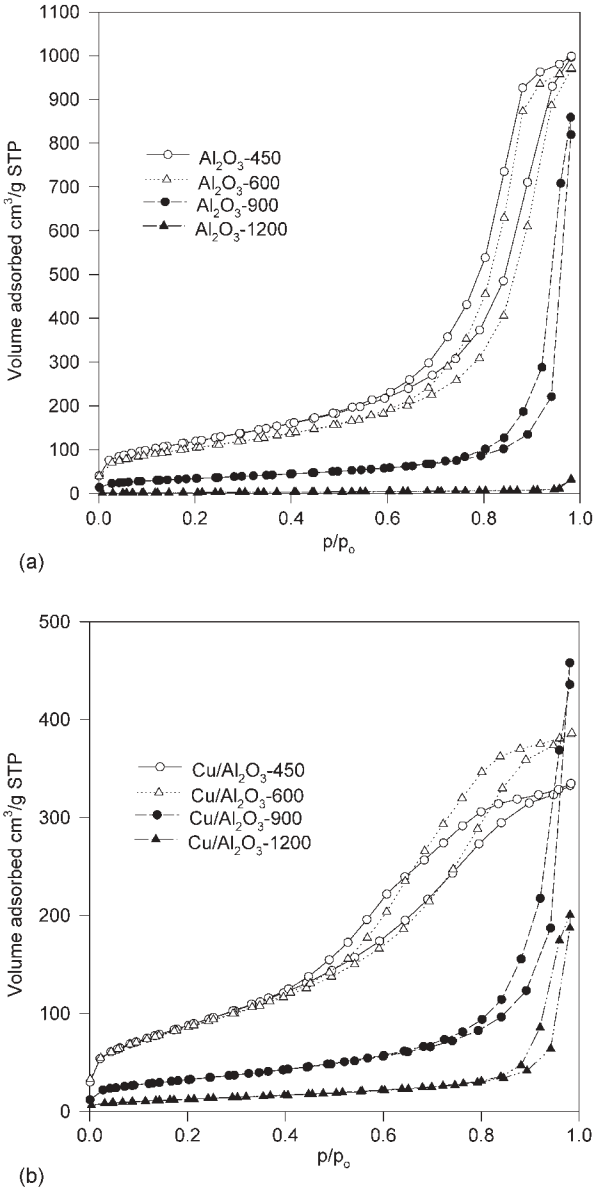

Figure 1. N_2 adsorption isotherms of Al_2O_3 supports and Cu/Al_2O_3 catalysts. (a) Support samples and (b) supported Cu/Al_2O_3 catalysts.

The sample Al_2O_3-1200 is obviously a nonporous solid showing the type II isotherm. A more quantitative comparison on the textural structure is presented in table 1. It is seen that calcination temperature exerts a great influence on the porous structure. The higher the temperature the lower the surface area and volume are. Very interestingly, the specific surface area and pore volume of Al_2O_3-450 are extremely high, over 400 m^2/g and 1.50 cm^3/g respectively. An increase in the calcination temperature up to 600 °C results in a little decrease in the surface area and pore volume. However, most of the pores were destroyed when the temperature was increased to 900 °C. And the Al_2O_3 sample becomes a nonporous solid at 1200 °C.

The mesoporous characteristics of the Al_2O_3 supports are confirmed by the pore-size distribution calculated from BJH method (figure 2(a)). The pore-size distributions of Al_2O_3-450 and Al_2O_3-600 are very similar, showing a two-mode peak centered at 10 nm and 12 nm, respectively. This suggests that the increase in heat treatment temperature from 450 to 600 °C led to a slight decrease in the surface area and pore volume, but little change in the pore-size distribution. In contrast, the pore-size distribution of Al_2O_3 was significantly changed by heat treatment at 900 °C. The peak around 12 nm disappears, and there is nearly a constant pore-size distribution from ca. 15 to 38 nm. The bigger pores ranging from 15 to 38 nm resulted from the pore coarsening and combination of the relatively small pores due to the sintering effect. A similar observation has been reported in the literature [14]. As also seen from the figure, Al_2O_3-1200 is almost a nonporous solid showing little pore-size distribution.

3.2. Phases of the Al_2O_3 supports

The XRD patterns of the Al_2O_3 supports are presented in figure 3. Both Al_2O_3-450 and Al_2O_3-600 are γ-Al_2O_3, with the three most intensive diffraction peaks at 37.5°, 46.0°, and 67.0°. The XRD pattern of Al_2O_3-900 is similar to those of Al_2O_3-450 and Al_2O_3-600, except that the peaks over Al_2O_3-900 are relatively sharper. This means that Al_2O_3-900 is still γ-Al_2O_3 but with an improved configuration order of atoms. Although the increase in heat treatment temperature of the Al_2O_3 supports could lead to the increase in particle size, which may in turn contribute to the sharpening of the peak, the following NMR results

Table 1
Pore structures of various Al_2O_3 supports and Cu/Al_2O_3 catalysts

	BET (m^2/g)	V_t (cc/g)	S_{micro}	V_{micro}	R (nm)
Al_2O_3-450	404.5	1.51	0	0	7.47
Al_2O_3-600	356.7	1.47	0	0	8.24
Al_2O_3-900	122.3	1.09	0	0	17.8
Al_2O_3-1200	13.4	0.002	0	0	0.72
Cu/Al_2O_3-450	293.8	0.51	0	0	3.47
Cu/Al_2O_3-600	290.0	0.59	0	0	4.07
Cu/Al_2O_3-900	116.9	0.57	0	0	9.75
Cu/Al_2O_3-1200	44.5	0.27	0	0	12.1

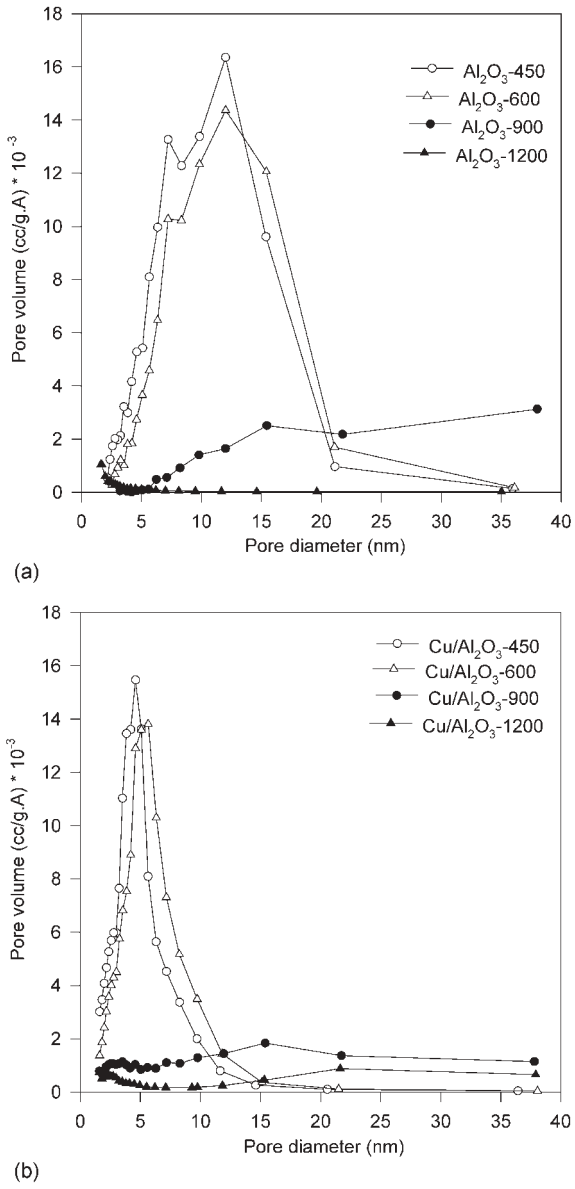

Figure 2. Pore-size distribution of Al_2O_3 supports Cu/Al_2O_3 catalysts. (a) Al_2O_3 supports and (b) Cu/Al_2O_3 catalysts.

show that the improved configuration order of atoms is the major contributor. The sample Al_2O_3-1200 is apparently α-Al_2O_3 with a further significantly improved configuration order of atoms.

More quantitative results were obtained from the NMR spectra of the four Al_2O_3 samples and are shown in figure 4. Al^{+3} ions at octahedral sites (Al_{Oh}) of the various samples are observed at ca. 5 ppm and Al^{+3} ions at tetrahedral sites (Al_{Td}) at ca. 60 ppm. The fractions of octahedrally coordinated Al^{+3} ions (Al_{Oh}) calculated from these spectra are displayed as functions of dehydration temperature in figure 5. The fraction of Al_{Oh} in Al_2O_3-450 is 0.693, which is close to the value of γ-Al_2O_3(0.75 ± 0.04) reported by John *et al.* [15]. The Al_{Oh} content in Al_2O_3-600 is only slightly improved compared to that of Al_2O_3-450, but a calcination

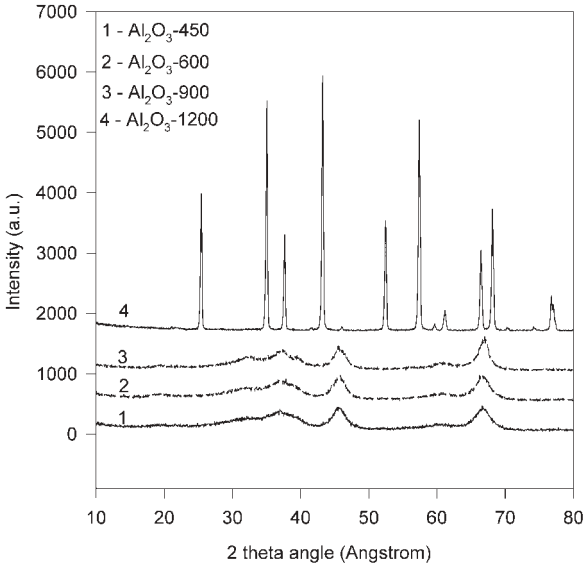

Figure 3. XRD patterns of Al_2O_3 samples.

temperature up to 900 °C increases the fraction of Al_{Oh} significantly. No Al_{Td} is left after the sample was calcined at 1200 °C, resulting in α-Al_2O_3 (also shown in the XRD patterns in figure 3).

Our results are in agreement with the previous reports [15–18], which show that at lower calcination temperatures a variety of phases are formed that are collectively known as γ-Al_2O_3. These phases represent various degrees of ordering of aluminium atoms in an essentially cubic close packing (CCP) of oxygen atoms, described as a defect spinel structure, since there are only 64/3 metal atoms arranged randomly in the 16 octahedral and 8 tetrahedral positions of that structure. This γ-Al_2O_3 is important technically because of its great adsorptive pore ("active alumina") and its catalytic properties. With the increase in calcination temperature,

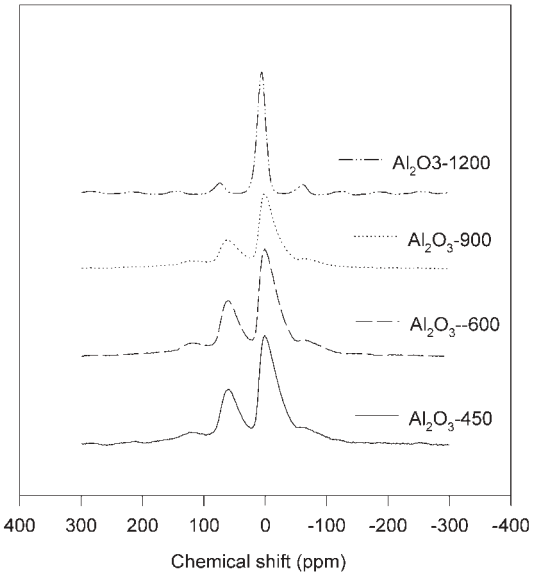

Figure 4. NMR spectra of Al_2O_3 samples.

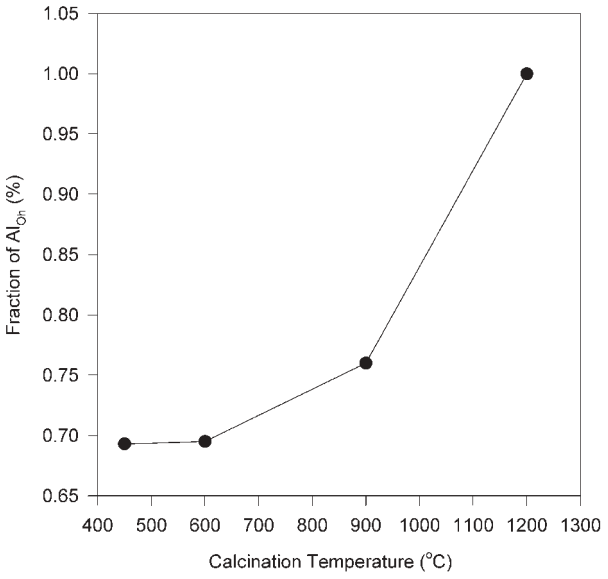

Figure 5. Ratio of octahedrally coordinated aluminum (Al_{Oh}) to total aluminium in the prepared Al_2O_3 calcined at different temperatures.

δ and θ phases can be formed. The former is a tetragonal spinel superstructure with a tripled *c*-axis where there are ordered vacancies in the octahedral sites. The latter is isostructural. In all the three forms, the oxygen atoms are of CCP or approximately so and the structural changes therefore involve only movements of the cations. α-Al_2O_3 can only be formed at very high temperature, and has a corundum structure with an approximately hexagonal close packing (HCP) array of oxygen atoms and Al^{3+} ions occupying two-thirds of the octahedral holes. In the present study, the shift of aluminium from tetrahedral to octahedral coordination with the increase in calcination temperature was clearly observed. As the ratios of Al_{Oh} in Al_2O_3-450 and Al_2O_3-600 are very close (both about 0.69) and the ratio of Al_{Oh} in Al_2O_3-900 is significantly improved to 0.763, Al_2O_3-900 is still γ-Al_2O_3 but may be at or close to the threshold point for δ-phase.

3.3. Pore structures of catalysts

The quantitative values of pore structures of Cu/Al_2O_3 catalysts are also presented in table 1. The impregnation of 5 wt% Cu on the supports reduced the surface areas and pore volumes of Al_2O_3-450 and Al_2O_3-600 significantly. This reduction can also be observed from the decreased adsorption volume in the adsorption isotherms of Cu/Al_2O_3-450 and Cu/Al_2O_3-600 (see figure 1(b)). The peaks of the pore-size distribution of these two catalysts become sharper and are shifted toward lower values (see figure 2(b)). This indicates that the loaded copper species are dispersed in pores reducing the pore size. The surface area and pore volume of Al_2O_3-900 was only slightly decreased after the impregnation of 5 wt% Cu. A comparison of the pore-size distributions of Cu/Al_2O_3-900 and Al_2O_3-900 shows that some of the pores above 20 nm are blocked by copper precursor. The impregnation of copper, however, produced some new mesopores in Al_2O_3-1200 since the surface area and pore volume of Cu/Al_2O_3-1200 are larger than that of the support Al_2O_3-1200. The pore-size distribution of Cu/Al_2O_3-1200 in figure 2(b) shows that the newly produced pores are mainly distributed above 20 nm.

The average loading of copper on catalysts in the form of wt%/100m^2/g-support are illustrated in table 2. Interestingly, the loading of copper in Cu/Al_2O_3-900 is 4.1 wt% Cu/100m^2/g-support, which is nearly the same as the threshold loading for the appearance of CuO (similar threshold loading despite different γ-Al_2O_3 samples) as reported in reference [1]. The copper loadings in Cu/Al_2O_3-450 and Cu/Al_2O_3-600 catalysts are much lower than the threshold because of their high surface areas, while the value on Cu/Al_2O_3-1200 is ninefold higher than the loading threshold because of its nonporous structure. This indicates that the major phases of copper species in Cu/Al_2O_3-450, Cu/Al_2O_3-600, and Cu/Al_2O_3-900 should be "surface spinel" and bulk $CuAl_2O_4$, not the bulk CuO, which is the major phase in Cu/Al_2O_3-1200. More information about the copper species can be confirmed from the following copper dispersion measured from N_2O chemisorption and UV–vis characterization.

3.4. Dispersion of copper on the catalysts

Dandekar and Vannice [12] have reported that the dispersion of copper on an Al_2O_3 support can be measured by N_2O chemisorption at 90 °C after the H_2 pretreatment at 300 °C. Under such conditions, the surface metallic copper sites produced by H_2 treatment can be oxidized into Cu_2O. At higher chemisorption temperatures or using other oxidants such as O_2, copper could be oxidized into CuO and some metallic copper in the bulk could also be oxidized. If the H_2 pretreatment temperature is below 300 °C, many surface copper

Table 2
The copper dispersion on Cu/Al_2O_3 catalysts

Catalysts	Cu/Al_2O_3-450	Cu/Al_2O_3-600	Cu/Al_2O_3-900	Cu/Al_2O_3-1200	Threshold value for appearance of bulk CuO [1]
Loading (Cu wt% /100 m^2/g-support)	1.24	1.42	4.1	37.0	4.0

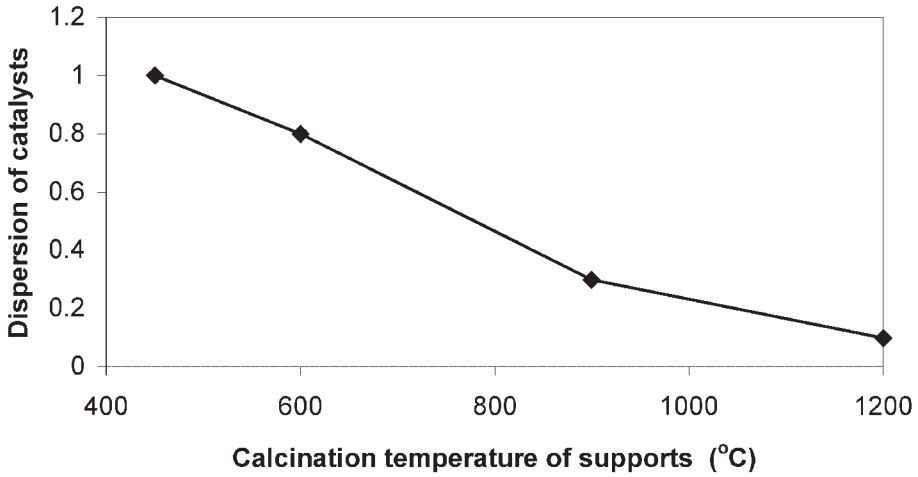

Figure 6. Oxygen adsorption and dispersion of Cu/Al_2O_3 catalysts.

species cannot be reduced into metallic copper. This method was used in this study and the copper dispersions ($D = Cu_{surface}/Cu_{total}$) were calculated by assuming a stoichiometry of $O : Cu^0_{surface} = 1:2$ from surface metallic copper sites to form Cu_2O [12]. Figure 6 presents the copper dispersions of the prepared catalysts. One can see that the copper dispersion on Cu/Al_2O_3-450 is perfect, nearly 1.0. This means that only ''surface spinel'' $CuAl_2O_4$ was formed in Cu/Al_2O_3-450 without bulk $CuAl_2O_4$. The copper dispersions of the catalysts decrease with the increase in calcination temperature of the corresponding supports. Cu/Al_2O_3-600 and Cu/Al_2O_3-900 should contain both ''surface spinel'' and bulk $CuAl_2O_4$ as the dispersion should be 1.0 if all the copper species were on the surface. The variation of copper dispersion was in line with the decreasing surface area of the supports. Evidently, the catalyst dispersions are strongly dependent on the surface area of the supports.

3.5. DR–UV–vis characterization

Figure 7 shows the diffuse reflectance spectra of the four catalysts before reaction. For Cu/Al_2O_3-900, the band at 750 nm is assigned to the octahedrally configured Cu^{2+} but slightly tetragonally distorted and the relatively weak band at 400 nm is due to Cu^+ [19]. The adsorption at 350 nm corresponds to the transition of charge transfer ($Cu^{2+} \rightarrow O^{2-}$). For both Cu/Al_2O_3-450 and Cu/Al_2O_3-600, Cu^+ was not observed, the band at 700 nm indicates that the octahedral configuration for Cu^{2+} is more tetragonally distorted than that in Cu/Al_2O_3-900. This is in line with the fact that there were more Al^{3+} ions in tetrahedral sites (Al_{Td}) in Al_2O_3-450 and Cu/Al_2O_3-600 than in Al_2O_3-900. The UV–vis results confirm the prediction above that no bulk CuO appeared in these three catalysts as the band at 600 nm, which indicates that the environment of Cu^{2+} is nearly square planar (like CuO), only appeared in the spectra of Cu/Al_2O_3-1200. Apparently, the copper species in Cu/Al_2O_3-1200 are mainly in the form of bulk like CuO. The band at 400 nm for Cu^+ is also observed over Cu/Al_2O_3-1200.

3.6. Catalytic activities of the catalysts

The N_2O conversions over the four catalysts prepared in this investigation were found to show high values at initial stage and then decrease gradually to reach a steady state after one-hour reaction. The selectivity for N_2 formation was 100% for four catalysts (not shown here), neither NO nor NO_2 was observed in the products. The activities over the four catalysts at the steady state are presented in figure 8. One can see that Cu/Al_2O_3 shows varying activity depending on the calcinations temperature. The N_2O conversion rate to N_2 over Cu/Al_2O_3-450 is substantially low and the activity is slightly improved over Cu/Al_2O_3-600. The

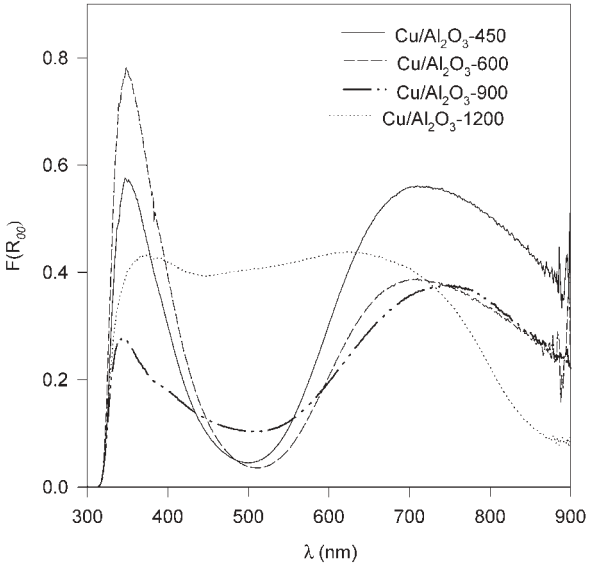

Figure 7. UV–vis spectra of supported Cu/Al_2O_3 catalysts.

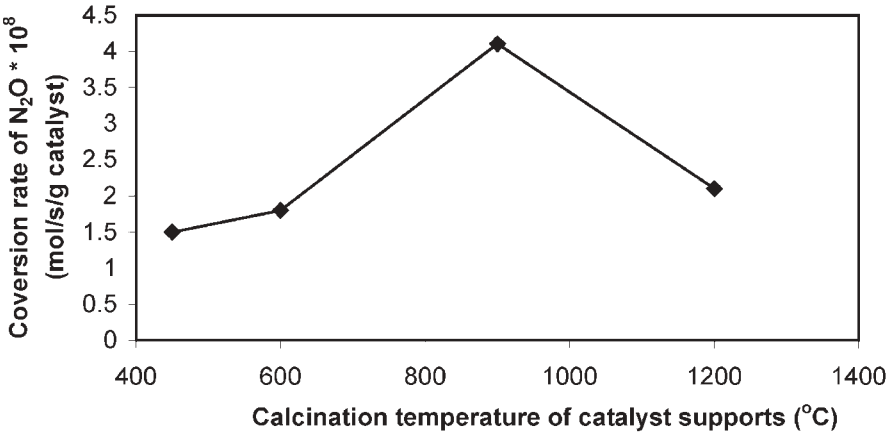

Figure 8. Activities of the Cu/Al_2O_3 catalysts (flow rate: 40.25 mL/min; reaction temperature = 475 °C; 1.02% N_2O/He).

activity of Cu/Al_2O_3-900 exhibits the highest value. Although the activity of Cu/Al_2O_3-1200 is greatly reduced, it still shows higher value than that over Cu/Al_2O_3-450 and Cu/Al_2O_3-600 catalysts. The difference of catalytic activities is believed to be closely related to the pore structures and phases of the supports, which will be discussed next.

4. Discussion

In this investigation, it has been demonstrated that the textural structure of mesoporous alumina can change significantly with the calcinations temperature. CuO supported on these supports will exhibit different phases and activities for N_2O dissociation. The copper species contains surface spinel and bulk $CuAl_2O_4$ and CuO. These species play different roles in the reaction. In the previous investigations, it has been proposed that the N_2O decomposition over metal oxides involved the participation of neighboring ions [20] and that an M-O-M system was assumed to constitute an active site. It can be rationalized by the so-called Zener double exchange [21], where two ions, differing by one oxidation state and bonded via an oxygen ion, can exchange an electron through the O_{2p} orbital leading to an average and easily adaptable oxidation state that facilitates the adsorption and desorption processes [20,22]. On the basis of these findings and the results in this study, we thus suggest two pathways for the decomposition reaction of N_2O over Cu/Al_2O_3 catalysts and the mechanism is shown in figure 9. Scheme I is for Cu/Al_2O_3-1200 and scheme II is for Cu/Al_2O_3-900, Cu/Al_2O_3-450, and Cu/Al_2O_3-600.

For Cu/Al_2O_3-1200, the environment of Cu^{2+} is nearly square planar (like CuO). Figure 7 clearly shows that Cu^+ (band at 400 nm) ions in Cu/Al_2O_3-1200 are produced after heat treatment, which are apparently active sites. Cu_2O, which contains Cu^+ ions, crystallizes in the cuprite structure formed by a bcc array of oxygen atoms with metal atoms inserted between two consecutive oxygen layers, in such a way that each oxygen atom is surrounded by a tetrahedron of copper ions [23]. Each metal atom is two coordinates, forming lineal Cu_2O units, as I-a in scheme I. The Cu^+ ions of I-a can be oxidized by dissociatively chemisorbing N_2O, resulting in I-b. I-b further accepts another oxygen from N_2O and becomes I-c. The desorption of O_2 from I-c releases two electrons, which reduce two Cu^{2+} ions into two Cu^+ ions.

It was reported that copper catalyst dispersed in Al_2O_3 is far more active than bulk CuO [8,20], and the

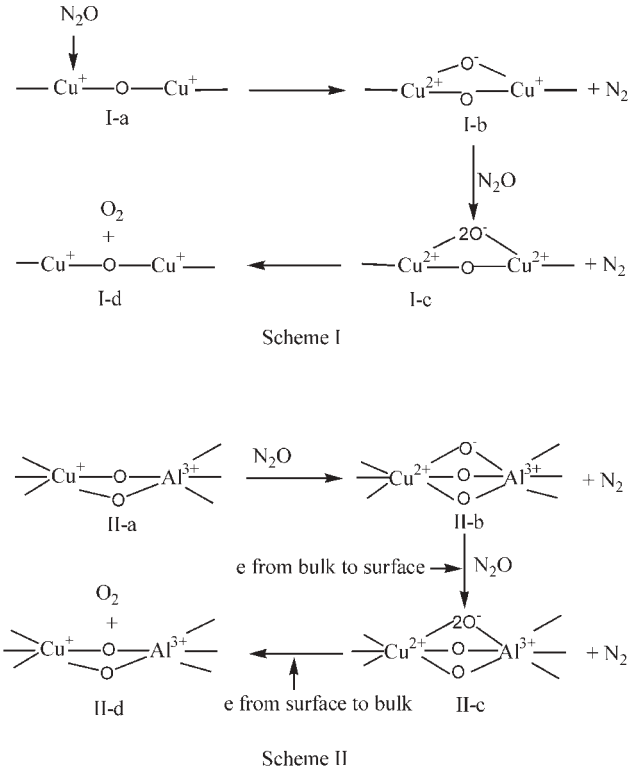

Figure 9. Proposed reaction mechanism schemes for N_2O decomposition.

present study also confirms that the activity of Cu/Al_2O_3-900 is much higher than that of Cu/Al_2O_3-1200. Copper catalyst is in the form of "surface spinel" and bulk $CuAl_2O_4$ in the former but something like bulk CuO in the latter. Therefore, the higher activity of Cu/Al_2O_3-900 must be related to the participation of Al^{3+}. From our UV–vis results in figure 7, octahedral copper ions predominated with perfect symmetry and more than 76% of Al^{3+} ions are also located in the octahedral sites in Cu/Al_2O_3-900. Therefore, similar to the reports in the literature on α-Cr_2O_3-Al_2O_3 catalyst [10], the double octahedral pair with one missing oxygen due to the heat treatment shown as model II-a, is suggested. Similar to Cu/Al_2O_3-1200, Cu^+ was also observed in Cu/Al_2O_3-900. There are two key differences between scheme II and scheme I. First, in scheme II, electron migrations from the bulk to the surface for taking the second oxygen from N_2O to form $2O^-$ during N_2O chemisorption and from surface to bulk during oxygen desorption are needed, while this is not necessary in scheme I. Second, in scheme II, one of the copper ion pairs is replaced by one Al^{3+}. As the Al^{3+} has no *d*-electron density to donate nor can it and since it cannot provide crystal field stabilization [10], the adsorbed oxygen will be more weakly held when one of the copper ions pair in scheme I is replaced by Al^{3+} as in scheme II. This makes the release of O_2 more readily in scheme II than in the scheme I. This is an important reason for the higher activity of Cu/Al_2O_3-900 compared with Cu/Al_2O_3-1200. Another important reason is that the low surface area of Al_2O_3-1200 results in the poor catalyst dispersion, thus significantly reducing the number of accessible active sites.

The mechanism for N_2O decomposition over Cu/Al_2O_3-450 and Cu/Al_2O_3-600 is similar to that over Cu/Al_2O_3-900 because of the commonly contained $CuAl_2O_4$ (either "surface spinel" or bulk). However, as discussed above, Cu/Al_2O_4-450 only contains "surface spinel" $CuAl_2O_4$ without bulk $CuAl_2O_4$. As Al_2O_3 is an insulator [10], electrons cannot be effectively transferred from the bulk to the surface or vice versa, resulting in the very low activity of Cu/Al_2O_3-450. Cu/Al_2O_3-600 contains some bulk $CuAl_2O_4$, thus resulting in a relatively higher electron conductivity and improved activity. Cu/Al_2O_3-900 with the threshold catalyst loading is nearly saturated with "surface spinel" and bulk $CuAl_2O_4$; both N_2O chemisorption and oxygen desorption are significantly improved because of the good electron conductivity. The poor electron conductivity in both Cu/Al_2O_3-450 and Cu/Al_2O_3-600 due to the lack of bulk $CuAl_2O_4$ is the key reason Cu/Al_2O_3-450 and Cu/Al_2O_3-600 have larger surface areas and better catalyst dispersion, but the activities are so poor. The higher ratio of tetrahedral aluminium and the more tetragonally distorted copper ions could also contribute to the lower activities of Cu/Al_2O_3-450 and Cu/Al_2O_3-600 as the O–M (M could be aluminium or copper) bonds are longer in octahedral structure than in the tetragonally distorted structures [1,24], but this may not be the major reason. The band at 400 nm for Cu^+ was not observed in the UV–vis spectra of Cu/Al_2O_3-450 and Cu/Al_2O_3-600 because of their low activities.

5. Conclusions

Mesoporous Al_2O_3 nanofibers were prepared and employed as supports for Cu/Al_2O_3 catalysts. These catalysts were then tested for N_2O reduction to N_2. The activity of Cu/Al_2O_3 varies with the structure and copper dispersion. Several copper species, surface spinel, bulk $CuAl_2O_4$, and CuO, are presented in Cu/Al_2O_3 catalysts. Cu/Al_2O_3-900 exhibits the highest activity due to the synergistic effect of surface spinel and bulk $CuAl_2O_4$. The former species acts as adsorption center (with the participation of aluminium) and the latter improves the electron transfer from bulk to surface during N_2O adsorption and from surface to bulk during oxygen desorption. For Cu/Al_2O_3-450 and Cu/Al_2O_3-600 catalysts, the electron conductivity is very poor because of the lack of bulk $CuAl_2O_4$, resulting in the very low activities. The bulk like CuO formed on Cu/Al_2O_3-1200 makes the oxygen desorption more difficult, resulting in its lower activity compared with Cu/Al_2O_3-900.

Acknowledgments

We acknowledge the assistance of Mr. C.Q. Lu in preparation of Al_2O_3 samples. We also thank Dr. Andrew Whittaker at the University of Queensland for NMR measurements and Prof. Jerry Lin at the University of Cincinnati for the discussion on mesoporous alumina. A financial support from the Australian Research Council is gratefully acknowledged.

References

[1] R.M. Friedman and J.J. Freeman, J. Catal. 55 (1978) 10.
[2] B.R. Strohmeier, D.E. Leyden, R.S. Field and D.M. Hercules, J. Catal. 94 (1985) 514.
[3] R.L. Chin and D.M. Hercules, J. Phys. Chem. 86 (1982) 360.
[4] M. Wu and D.M. Hercules, J. Phys. Chem. 83 (1979) 2003.
[5] R. Hierl, H. Knözinger and P. Urbach, J. Catal. 69 (1981) 475.
[6] S.F. Tikhov, V.A. Sadykov, G.N. Kryukova, E.A. Paukshtis, V.V. Popovskii, T.G. Starostina, G.V. Kharlamov, V.F. Anufrienko, V.F. Poluboyarov, V.A. Razdobvarov, N.N. Bulgakov and A.V. Kalinkin, J. Catal. 134 (1992) 506.
[7] W.P. Dow, Y.P. Wang and T.J. Huang, J. Catal. 160 (1996) 155.
[8] K. Shimizu, H. Maeshima, A. Satsuma and T. Hattori, Appl. Catal. B 18 (1998) 163.
[9] K.W.Yao, S. Jaenicke, J.Y. Lin and K.L.Tan, Appl. Catal. B 16 (1998) 291.
[10] T.A. Egerton, F.S. Stone and J.C.Vickerman, J. Catal. 33 (1974) 307.

[11] B.C. Lippens and J.H. deBoer, J. Catal. 4 (1965) 319.
[12] A. Dandekar and M.A. Vannice, J. Catal. 178 (1998) 621.
[13] E. Garbowski and H. Praliaud, in *Catalyst Characterization: Physical Techniques for Solid Materials*, B. Imelik and J.C. Bedrine (eds) (Plenum, New York, 1994) p. 61.
[14] S.J. Gregg and K.S.W. Sing, *Adsorption, Surface Area and Porosity*, 2nd ed. (Academic Press, New York, 1982).
[15] C.S. John, N.C.M. Alma and G.R. Hays, Appl. Catal. 6 (1983) 341.
[16] S.J. Wilson and J.D.C. McConnell, J. Solid State Chem. 34 (1980) 315.
[17] B.C. Lippens and J.H. de Boer, Acta Crystallogr. 17 (1964) 1312.
[18] A.F. Wells, *Structural Inorganic Chemistry*, 5th ed. (Oxford University Press, New York, 1984) pp. 544 and 552–553.
[19] H. Praliaud, S. Mikhailenko, Z. Chajar and M. Primet, Appl. Catal. B 16 (1998) 359.
[20] F.K. Kapteijn, J. Rodriguez-Mirasol and J.A. Moulijn, Appl. Catal. B 9 (1996) 25.
[21] L.G. Tejuca, J.L. Fierro and J.M.D. Tascon, Adv. Catal. 36 (1989) 237.
[22] D.K. Chakrabarty and D.Y. Rao, React. Kinet. Catal. Lett. 33 (1987) 131.
[23] E. Ruiz and S. Alvarez, Phy. Rev. B 56 (1997) 7189.
[24] C. Angeletti, F. Pepe and P. Porta, J. Chem. Soc., Faraday Trans. 1 I-51 (1977) 1595.